Visual high-throughput screening for developing fatty acid amide hydrolase natural inhibitor based on an enzyme-activated fluorescent probe

Xiangge Tian, [†,‡,#] Tao Liu, [§,#] Lu Li, [†,#] Bo Shao, [∥] Dahong Yao, [∓] Lei Feng,[*†] Jingnan Cui, [§] Tony D. James,[*⊥] and Xiaochi Ma[*†,‡]

[†] Jiangsu Key Laboratory of New Drug Research and Clinical Pharmacy, Xuzhou Medical University, 209 Tongshan Road, Xuzhou, 221004, Jiangsu, China;

[‡] College of Integrative Medicine, The National & Local Joint Engineering Research Center for Drug Development of Neurodegenerative Disease, College of Pharmacy, Dalian Medical University, Dalian 116044, China;

[§] State Key Laboratory of Fine Chemicals, Dalian University of Technology, Dalian 116024, China;

[∥] Zhendong Pharmaceutical Research Institute Co. Ltd.; Changzhi 047100, China;

[∓] Department of Pharmacology, School of Medicine, Shenzhen University, Shenzhen 518060, China;

[⊥] Department of Chemistry, University of Bath, Bath, BA2 7AY, United Kingdom.

[*] Corresponding Author: Xiaochi Ma, Tony D. James and Lei Feng (E-mail: maxc1978@163.com, t.d.james@bath.ac.uk and leifeng@dmu.edu.cn).

ABSTRACT: Fatty acid amide hydrolase (FAAH) is an important drug target for the treatment of many disease related conditions such as pain, inflammation and mood disorders due to its vital role in the metabolism of endocannabinoid. In our present work, a FAAH-activated fluorescent probe named **THPO** was developed which possessed high selectivity and excellent sensitivity for FAAH in complex systems. Critically, its metabolite **AHPO** has long excitation and emission wavelengths and high fluorescence quantum yield which are necessary for monitoring the activity of FAAH in living systems. In addition, a visual high-throughput screening method for FAAH inhibitors was established using **THPO** which resulted in the discovery of an efficient natural inhibitor Neobavaisoflavone that was identified from 68 traditional herbal medicines. These results indicated that **THPO** can be used as a molecular tool for the rapid evaluation of FAAH activity in complex systems as well as providing an effective approach to screen FAAH inhibitors and providing a boost for the discovery of therapeutic agents toward FAAH related diseases.

INTRODUCTION

Fatty acid amide hydrolase (FAAH) is a key bioactive protein, it belongs to a large family of enzymes that shares a highly conserved 130 amino acid motif designated the "amidase signature" sequence and has an extensive expression in the brain and some other tissues.[1-5] FAAH catalyzes the hydrolysis of some biologically active amides and agonists of the peroxisome proliferator-activated receptors.[6] It is mainly responsible for the inactivation of fatty acid ethanolamides (FAEs), in particular, catalyzing the hydrolysis reaction of arachidonoylethanolamide (AEA) to arachidonic acid and ethanolamine terminating signal transduction.[7-9] AEA is the most comprehensively investigated endocannabinoid which is involved in a variety of biological functions related to pain and inflammation.[10,11] Thus, FAAH plays an important role in various conditions for instance: inflammation, neuropathic pain, nonsmall cell lung cancer and Alzheimer's disease. All these diseases are related to the hydrolysis process of AEA, due to the powerful ripple effect mediated by AEA, and AEA not only modulates nociception, but also attenuates neutrophil migration and immue-cell recruitment during inflammation, through activation of CB1 and CB2 receptors.[9,12-14] Therefore, the discovery of 'classical' FAAH inhibitors as well as the development of molecular tools for rapidly evaluating the FAAH activity in complex systems are urgently required. Such molecular tools would facilitate rapid and accurate measurement of FAAH activity and further determine efficient inhibitors for treatment of various diseases.[15-19] Recently, some FAAH inhibitors were designed and developed such as PF-04457845, URB597, URB524, and BMS-1.[20-22] Though these inhibitors exhibited good activity in cell and animal models, they all exhibited significant side effects such as the failure of PF-04457845 (FAAH inhibitor) in the Phase II study on osteoarthritic pain.[23] Therefore, nontoxic and effective FAAH inhibitors as potential medicines are urgently needed for clinical use; all of these studies require an effective method for the high-throughput screening of FAAH inhibitors.

Fluorescence techniques have been widely used for enzyme-related drug screening and disease diagnosis with many advantages including sensitive, real-time detection, high spatiotemporal resolution, and noninvasive monitoring efficacy in various living systems as well as high-throughput screening capability.[24-30] Recently, some fluorescent probes for FAAH have been developed,[31-35] however, challenges including short emission wavelength has limited their applicability in complex biological systems for screening inhibitors. Additionally luciferase-dependent probes require luciferase expression in complex biological systems, importantly; it was hardly to distinguish the final inhibition activity was dependent on inhibiting the FAAH or luciferase, all of which limits the practical applications of these probes.[34,35] Therefore, developing long-wavelength fluorescent probe for selectively and sensitively monitoring endogenous FAAH activity in complex biological systems and establishing visual high-throughput screening methods for the discovery of FAAH inhibitors are urgently needed.

Herein we developed a fluorescent substrate (**THPO**) for FAAH (**Scheme 1**), by introducing arachidonic acid as a specific recognition moiety for FAAH into the skeleton of 7-amino-3*H*-phenoxazin-3-one (**AHPO**). As expected, **THPO** possesses some prominent advantages: firstly, the metabolite

AHPO not only has red-emission wavelength ($\lambda_{ex}/\lambda_{em}$ = 550/592 nm) but also possesses high fluorescence quantum yield; secondary, **THPO** exhibited high specificity and sensitivity toward FAAH among various hydrolase enzymes; thirdly, **THPO** can be applied for monitoring and imaging of FAAH in living cells, as well as establishing a visual high-throughput screening platform for novel FAAH inhibitors from herbs. In a word, **THPO** could act as a promising tool in the rapid evaluation of FAAH activity in complex systems, and the screening of FAAH inhibitors for the development of clinical agents.

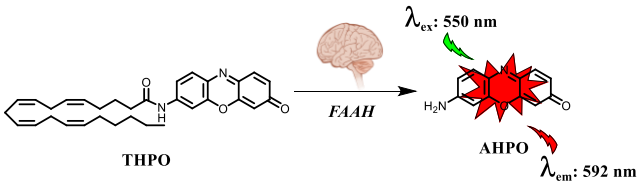

Scheme 1. The mechanism of **THPO** catalyzed by FAAH.

EXPERIMENTAL SECTION

Materials and instruments. Fatty acid amide hydrolase used in this experiment was expressed in 293T cells. SH-SY5Y cells were purchased from American Type Culture Collection. Trypsin (Try), Lysozyme (Ls), Proteinase K (PaK), Carbonic anhydrase (Cas), *N*-acetyl glucosaminidase (NAG), Proline aminopeptidase (PAP), *β*-Galactosidase (*β*-Gla), Dipeptidyl Peptidase 4 (DPP4), *β*-Glucosidase (*β*-Glc), *β*-Glucuronidase (*β*-Glu), Lipase, and were all obtained from Sigma-Aldrich. Glycine, Glutamate, Arginine, Glutamine, Tryptophan, Serine, Glutathione, Myristic acid, Tyrosine, Cysteine, Glucose, and lysine were purchased from Shanghai Yuanye (Shanghai, China). URB597 was purchased from Selleckchem. BCA Protein Quantitation Kit was purchased from Beyotime (Shanghai, China). All other reagents and solvents used were of the highest grade commercially available. All fluorescence analysis were conducted on Synergy H1 Microplate Reader (Bio-Tek). NMR spectra were required using Bruker-600. HRMS detection was measured on G6224A TOF MS. The hydrolysis supernatants were determined by HPLC-UV analysis (Waters e2695 equipped PDA Detector). The HPLC fractions of *Psoralea corylifolia Linn.* were obtained by HPLC (Waters 2767 Sample Manager with Waters 2489 UV Detector).

***Synthesis pathway for THPO*.** The starting material of 7-amino-3*H*-phenoxazin-3-one (**AHPO**) was prepared following the reported procedure.[36] (**Figure S1**). Arachidonic acid (72 mg, 0.24 mmol), EDCI (136 mg, 0.72 mmol) and DMAP (58 mg, 0.48 mmol) were dissolved in CH_2Cl_2 (5 mL). Then a solution of **AHPO** (50 mg, 0.24 mmol) in THF (5 mL) was added slowly. The resulting mixture was stirred at room temperature for an additional 24 h, and then the solvent was removed under reduced pressure, the crude product was purified by silica gel chromatography (ethyl acetate/petroleum ether = 1:2) to obtain the product as red solid (16 mg, 13% yield). ^{1}H NMR (600 MHz, DMSO-d_6) δ 10.53 (s, 1H), 7.96 (d, J = 2.2 Hz, 1H), 7.78 (d, J = 8.7 Hz, 1H), 7.53 (d, J = 9.8 Hz, 1H), 7.49 (dd, J = 8.8, 2.2 Hz, 1H), 6.79 (dd, J = 9.8, 2.1 Hz, 1H), 6.29 (d, J = 2.1 Hz, 1H), 5.56 – 5.11 (m, 8H), 2.76 (ddd, J = 26.5, 12.1, 6.2 Hz, 6H), 2.40 (t, J = 7.3 Hz, 2H), 2.10 (dd, J = 13.8, 6.8 Hz, 2H), 1.98 (dd, J = 14.1, 7.0 Hz, 2H), 1.73 – 1.63 (m, 2H), 1.33 – 1.13 (m, 6H), 0.83 (t, J = 7.0 Hz, 3H).^{13}C NMR (150 MHz, DMSO-d_6) δ184.76, 171.51, 149.19, 145.31, 143.80, 143.04, 134.29, 133.27, 130.10, 129.29, 128.60, 128.47, 127.74, 127.44, 127.35, 127.15, 127.02, 126.85, 115.77, 105.18, 104.05, 39.44, 35.25, 30.26, 28.09, 25.96, 25.48, 24.61, 24.56, 24.02, 21.36, 13.31. HRMS (ESI positive) calcd for $[M+H]^+$ 499.2955, found 499.2947. All the NMR and HRMS data were shown in **Figure S2-4**.

Expression, purification and characterization of recombinant FAAH. The vector for FAAH production, FAAH-HIS pCDH-PURO was constructed with the primers FAAH_F (5'–GATTCTAGAGCTAGCGAATTCGCCACCATGGTGCAGT ACGAGCTG–3'), FAAH_R (5'–GCCGCGGATCCGATTTAAATTTAGTGGTGGTGGTGGT GGTGCTCGAGGGATGACTGCTTTTCAGGGGTC–3'), and the HIS tag was attached to the c-terminal of the target gene. After verification of the sequence, the recombinant plasmid was transfected into 293T cells, the cells were harvested by scraping 48 h post-transfection, disrupted by sonication in an ice bath and the cell debris was removed by centrifugation at 10,000 *g* and 4 °C for 10 min. Next, the recombinant FAAH was purified as the previous reports.[37,38] Briefly, the cleared supernatant was immediately applied to 1 mL of Ni-NTA resin loaded in a column which was pre-equilibrated with binding buffer. The resin was subsequently washed with 10 mL washing buffer. Elution was carried out with 5 mL elution buffer. The protein purification was performed under the flow rate of 1 mL/min and the temperature of 4 °C. Finally, the recombinant protein was desalted in desalting buffer by 3 cycles of concentration and obtained using Amicon Ultra-30K and stored at −80 ºC. Protein purity was confirmed by SDS-PAGE to be > 80% and protein concentration for all studies was determined by the Protein Quantitative Kit. All the Protein purity data were shown in **Figure S5-6**.

Incubation conditions and analysis method. In order to characterize the spectral characteristic of **THPO** and its fluorescence response toward FAAH, the whole system with a total volume of 200 μL containing Tris-EDTA-BSA buffer (125 mM Tris-Hcl, 1 mM EDTA, 0.1% BSA, pH = 8), **THPO** and FAAH. In brief, **THPO** (10 μM) was added after preincubation of FAAH in the standard system at 37 °C for 3 min. Organic solvent (DMSO) was not more than 1% (*v/v*). The incubation reaction was performed at 37 °C for 30 min, and then terminated by adding 100 μL ice-cold acetonitrile, followed by centrifugation for 20 min at 4 °C at 20,000 *g*.[29] The supernatant was subjected to Synergy H1 Reader (Bio-Tek) and HPLC analysis. Additionally, the control experiment without FAAH was performed in a similar way to make sure that metabolite formation was FAAH-dependent. We also explored the relationship of fluorescence intensity change of **THPO** toward FAAH following the change of enzyme concentration and the reaction time, respectively. All assays were performed three times.

***Screening the selectivity of THPO*.** The selectivity of **THPO** toward FAAH was evaluated, briefly, **THPO** was incubated with various enzymes including Try, Ls, PaK, Cas, NAG, *β*-Gla, *β*-Glc, *β*-Glu, PAP, Lipase and DPP4 in the standard incubation

system at 37 °C for 30 min with the final enzyme concentration at 15 μg/mL, respectively. Furthermore, we also examined the influence of common metal ions such as positive ions K^+, Ca^{2+}, Zn^{2+}, Fe^{3+}, Mn^{2+}, Sn^{2+}, Mg^{2+}, Cu^{2+}, Ni^+, Ba^{2+}, Na^+; negative ions like NO_3^-, CO_3^{2-}, SO_4^{2-}, and some amino acids: Serine, Glutamate, Glucose, Glutamine, Glycine, Glutathione, Tyrosine, Arginine, Lysine, Cysteine, Tryptophan, and Myristic acid on the fluorescence intensity of **THPO** and **AHPO** in the standard incubation system with the final concentration of 10 μM, respectively[29]. Finally, the supernatant was subjected to Synergy H1 Reader for analysis and all assays were performed three times.

Kinetics Study. The kinetic parameters are very important for the application of the probe and also illustrate the affinity of the substrate towards the enzymes. Therefore, we conducted the kinetic study to estimate the kinetic constants of **THPO** for FAAH. In brief, **THPO** (0 – 100 μM) was incubated with FAAH (15 μg/mL) for 30 min. The incubation times and protein concentrations were selected in the linear range.[29] The apparent K_m and V_{max} values were calculated from nonlinear regression analysis of experimental data according to Michaelis-Menton (1).

$$V = V_{max}\frac{[S]}{K_m+[S]} \quad (1)$$

The V_{max} represents the maximal catalytic velocity and K_m is the substrate concentration with the half-maximal rate which represents the affinity of **THPO**. Kinetic constants were obtained using GraphPad Prism 6 and produced as the mean ± SD of the parameter estimate.[29]

Chemical Inhibition. To further validate the specific property of **THPO** toward FAAH, we performed chemical inhibition experiments. **THPO** (10 μM) was incubated with various hydrolase inhibitors including Baicalin (100 μM), LPA (100 μM), KCZ (100 μM), Biochain A (1 μM) and URB597 (10 nM) in the standard incubation system at 37 °C for 30 min with the final brain S9 concentration at 20 μg/mL, respectively. Finally, the supernatant was subjected to Synergy H1 Reader for analysis and all assays were performed three times.

The fluorescence imaging of FAAH in living cells. Firstly, cytotoxicity was evaluated using the CCK-8 assay (Roche Diagnosis, Indianapolis, IN). In brief, SH-SY5Y cells were seeded in a 96-well plate with the final concentration of 5×10^3 cells were seeded in each vial. Then FBS free culture medium containing various concentrations of **THPO** was added (0, 1, 2, 5, 10, 20, 50 and 100 μM), the control group used blank solvent without **THPO**. After 24 hours incubation, the culture medium was discarded and FBS free culture medium with 10% (*v/v*) CCK-8 was added.[39] After one-hour incubation, the plate was detected at 450 nm in a Synergy H1 Reader (Bio-Tek). Cell viability of the samples without **THPO** was considered to be 100%.[29] Next, the imaging ability of **THPO** in SHSY-5Y cells was evaluated. Briefly, SHSY-5Y cells were cultured in RPMI-1640 medium with fetal bovine serum (FBS) of 10% in an atmosphere of 5% CO_2 at 37 °C. Next, the cells were reseeded on 10 mm coverslip in 6-well plate at a concentration of 2×10^5 cells mL^{-1}. After SHSY-5Y cells were attached, the adherent cells were incubated with **THPO** (20 μM) for 60 min at 37 °C in a 5% CO_2 incubator, additionally another group was pretreated with URB597 (5 μM, prepared in medium containing 5% FBS) for 30 min and then incubated with **THPO** under the same condition mentioned above. Then, the residual **THPO** was removed and imaged using a confocal microscope (Leica TCS SP8) with the excitation laser at 561 nm and acquisition wavelength at 575 – 630 nm.

Visual high-throughput screening of FAAH inhibitor from herbal medicines. In order to investigate the inhibitory effects of natural products of herbal drugs towards FAAH, a high-throughput screening method was developed using **THPO** *in vitro*. Due to the abundant expression of FAAH in rat brain,[8,11] and our results indicated that the inhibition activity of URB597 (classic selective inhibitor for FAAH) in Brain S9 was very close with the recombinant FAAH (IC_{50}: 7.84 ± 0.031 nM *vs* 3.45 ± 0.001 nM). Thus, Rat brain S9 (20 μg/mL) was used as the enzyme resource in the high-throughput screening. Firstly, the extracts of 68 kinds herbal medicines were obtained as follows (Table S1): each herb (5 g of dried plant sample) was accurately weighted and ground to fine particles, and then passed through a 40-mesh screen. After which, they were extracted with 95% ethanol (100 mL) by ultrasonication at room temperature for 60 min, respectively; and the extraction process was repeated for three times, and the extracts were filtered *in vacuo* and then collected and evaporated. Then, the dried extract was dissolved in DMSO 20 mg/mL as a stock solution, these extracts of 68 herbal medicines were added to our standard system in the presence of **THPO** (10 μM) at the finial concentration of 20 μg/mL (containing less than 1% DMSO), respectively. The same volume of DMSO instead of herbal extract as the control group was added in the same incubation system. Finally, after incubation at 37 °C for 30 min, 100 μL ice-cold acetonitrile was added to terminate the reaction. The supernatant was transferred to a 96-well plate and imaged in GE Typhoon FLA9500 with an excitation laser of 532 nm equipped with the emission filter of 570 ± 10 nm. The residual activity was analyzed semi-quantitatively by fluorescence imaging. Meanwhile the samples were also tested by Synergy H1 reader (Bio-Tek), and the residual activity was calculated, the control group without herb medicines was considered as 100%.

Isolation and identification of the key inhibitory compound of Psoralea corylifolia Linn. toward FAAH. The fruits of *Psoralea corylifolia Linn*. (2 kg) were powdered and extracted using ethanol reflux (10 L × 3). After the evaporation of ethanol, the HPLC fractions of extracts were obtained using an efficient HPLC method (the mobile phase consisted of 10% acetonitrile + 90% trifluoroacetic acid water (A) and acetonitrile (B) at a flow rate of 10 mL/min. The following gradient condition was used: 0 – 10 min 75% A; 10 – 50 min 75% – 10% A; 50 – 55 min 10% – 75% A; 55 – 75 min 75% A.), several fractions were collected, and then the inhibitory effects of these fractions were evaluated by the above method using **THPO** (10 μM) and Rat Brain S9 (20 μg/mL). Additionally, in order to confirm the inhibitory nature of the fractions on the FAAH, the inhibition activity of the 13 fractions on the classic hydrolysis reaction of AEA which in catalyzed by FAAH in human was also performed. In brief, Fractions (2.5 μg/mL) and cannabinoid (10 μM) was incubated with rat brain S9 (40 μg/mL) in the standard

incubation system at 37 °C for 60 min. Finally, the supernatant was subjected to LC-MS for analysis. The HPLC analysis method was as follows: the mobile phase consisted of acetonitrile (B) and 0.1% formic acid aqueous solution (C) at a flow rate of 0.5 mL/min. The following gradient condition was used: 0 – 7 min 20% B The negative mode was used with the following values: AA (Q1→Q3 : 303.0 → 303.0). **Fr. 5** was confirmed as a potent inhibition fraction and the key compound in **Fr. 5** was isolated and purified by the HPLC (60% Methanol: 40% trifluoroacetic acid water) equipped with DAD detector and ODS column (Agela Innoval ODS-2, 4.6 mm × 250 mm, 5 μm), the potential inhibitor was purified from the bioactive fraction using preparative HPLC as **L-BGZ**. Subsequently, the IC_{50} values of Neobavaisoflavone and the previously reported natural inhibitor Biochanin A for **THPO** were determined. Inhibitors (0 – 20 μM) and **THPO** (10 μM) was incubated with FAAH (20 μg/mL) for 30 min. Finally, the supernatant was subjected to Synergy H1 Reader for analysis. IC_{50} refers to the inhibitor concentration at which residual activity reaches 50%. Data were obtained using GraphPad Prism 6 and all tests were repeated three times.

Molecular docking. Discovery Studio 3.5 was employed by docking the ligands to FAAH1. The structure of human FAAH1 was built by homologous modeling based on the template of Rattus norvegicus FAAH1 (PDB code: 2WJ1) [40]. The active binding site was defined according to the reference ligand with a radius of 8.5 Å. The protein structure was processed by adding hydrogen atoms, removing water, and assigning Charmm forcefield. The gold score was selected as the score function, and the other parameters were set as default. A maximum of 20 conformations were generated. 30 ligand poses were allowed to be saved with a minimum RMSD between final poses of 0.50 Å [41].

RESULTS AND DISCUSSIONS

Spectral properties of THPO toward FAAH. Firstly, human recombinant expression FAAH was obtained in HEK293T cells which overexpressed FAAH. Then, after incubating with FAAH, the spectral properties of **THPO** exhibited a significant change, as shown in **Figure 1A-B, and Figure S7**; a remarkable enhancement of the absorption at 560 nm was detected, followed by a significant increase in the fluorescence signal at 592 nm. The incubated samples were analyzed using HPLC, as shown in **Figure S8**, a new chromatographic peak was observed after incubating with FAAH (**THPO** 10 μM was incubated with FAAH (25 μg/mL) in the standard incubation system at 37 °C for 60 min.), electrospray ionization (ESI) mass spectra of the reaction product resulted in $[M+H]^+$ ion peak at *m*/*z* 213.2 which was identified as **AHPO**. Additionally, the reaction exhibited good enzyme linear range from 0 – 45 μg/mL (**Figure 1**) and a linear time-dependent

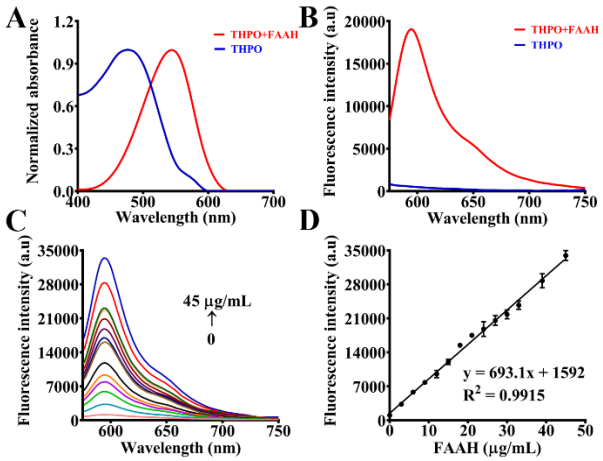

Figure 1. The absorbance (A) and fluorescence (B) spectra response of **THPO** after incubating with FAAH (25 μg/mL) at 37 °C for 30 min; The fluorescence spectra response (C) and liner relationship (D) of fluorescence intensity at 592 nm toward the increasing of the concentration of FAAH.

(**Figure S9**). As shown in **Figure S10**, the influence of pH on the fluorescence intensity of **THPO** and **AHPO** indicated that the metabolite **AHPO** exhibited a stable fluorescence emission under physiological conditions. All the above results clearly demonstrated that the fluorescence of **THPO** displayed turn-on when metabolized by FAAH.

Screening the selectivity of THPO toward FAAH. Next, the specificity for **THPO** among some major human metabolic enzymes was investigated. As shown in **Figure S11A**, **THPO** was a selective substrate for FAAH and displayed a significant fluorescence response, while other enzymes including Try, Ls, PaK, Cas, NAG, *β*-Gla, *β*-Glc, *β*-Glu, PAP, lipase, and DPP4 had no fluorescence response. Additionally, **THPO** and **AHPO** could not be influenced by common endogenous substances, metal ion and some negative ions including: GSH, Lys, Gly, Glucose, Tyr, Myristic acid, Gln, Cys, Trp, Ser, Glu, Arg, and Na^+, Ca^{2+}, K^+, Zn^{2+}, Ni^+, Mn^{2+}, Mg^{2+}, Fe^{3+}, Ba^{2+}, Cu^{2+}, Sn^{2+}, CO_3^{2-}, SO_4^{2-}, and NO_3^- (**Figure S11B, S12**).

Kinetics Study. A kinetic analysis was performed to obtain the characteristic of **THPO** for detecting FAAH. As shown in **Figure S13**, the metabolism of **THPO** mediated by FAAH exhibited Michaelis-Menton kinetics model and the K_m was 1.84 ± 0.14 μM, V_{max} = 0.227 ± 0.003 nmol/mg/min. The kinetic evaluation indicated that **THPO** had a high affinity toward FAAH which made it efficient in detecting FAAH activity in complex biological samples. Importantly, after introducing URB597 and Biochanin A as the highly selective inhibitors for FAAH, the fluorescence response could be significantly blocked, while other inhibitors such as Loperamide hydrochloride (LPA, the selective inhibitor for CES2), Ketoconazole (KCZ, CYP3As inhibitor), and baicalin (*β*-Glucuronidase inhibitor) produced only slight inhibitory effects on the fluorescence response (**Figure S14**). All the above results fully demonstrated that **THPO** can serve as a highly sensitive and selective fluorescent tool to measure FAAH activity.

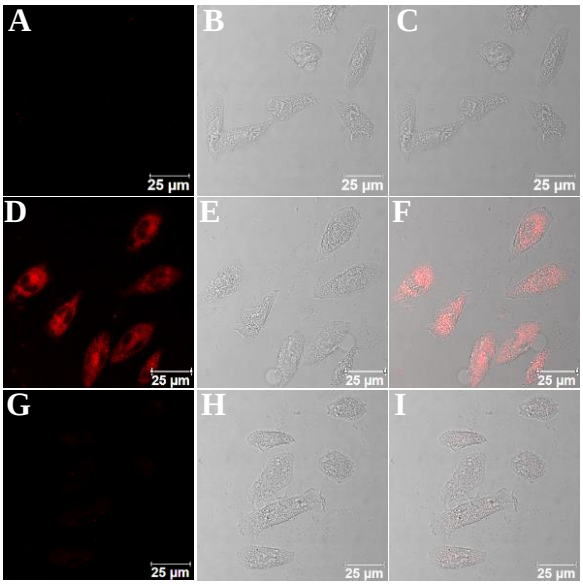

Figure 2. Confocal fluorescence images of FAAH in living cells. (**A – C**) the confocal fluorescence background images of SHSY-5Y at 575 – 630 nm with 561 nm excitation; (**D – F**) the confocal fluorescence images of SHSY-5Y cells after incubating with **THPO**; (**H – J**) the confocal fluorescence images at of SHSY-5Y cells pretreated with URB597 and stained with **THPO**. Scale bars 25 μm.

Fluorescence imaging of FAAH in living cells. FAAH is expressed in nerve cell in brain, and mediates the hydrolysis of cannabinoids.[8, 11] Therefore, in the current study; the fluorescence imaging of FAAH in SHSY-5Y cells was evaluated. Firstly, **THPO** displayed no cytotoxicity for SHSY-5Y up to 100 μM (**Figure S15**). Then, after incubating **THPO** (20 μM) with SHSY-5Y cells for 1 h at 37 °C, the cells displayed significant fluorescence intensity in the red channel (575 – 630 nm), while the group pretreated with URB597 (5 μM) had weak fluorescence response (**Figure 2**). These results indicated that **THPO** had good cell permeability and specificity for real-time monitoring of FAAH activity in living cells. These results indicated that **THPO** could serve as an efficient and selective tool for detecting FAAH activity in complex biological systems.

Visual high-throughput screening of FAAH inhibitor from herbal medicines. FAAH has been determined as a suitable drug target in the treatment for many disease related conditions including pain, inflammation and mood disorders. [3,16,18] In order to discover suitable lead compounds for further study, we screened for FAAH inhibitors from herbal medicines. As shown in **Figure 3A-C**, 68 kinds of herbal medicines were used for the visual high-throughput screening approach (**Table S1**), among which *Psoralea corylifolia Linn.* (herb. **41**) exhibited significant inhibition at 20 μg/mL. While other herbs including rhizoma alismatis, motherwort, ginkgo leaf, liquorice displayed only slight inhibitory effect. Thus, *Psoralea corylifolia Linn.* was chosen for further study. These results indicate that **THPO** can be used as a promising tool for visual high-throughput screening of FAAH inhibitors. Next, as shown in **Figure 4**, 13 fractions were collected according to the HPLC chromatogram of *Psoralea corylifolia Linn.* and their inhibitory effects toward FAAH were evaluated using the method mentioned above.

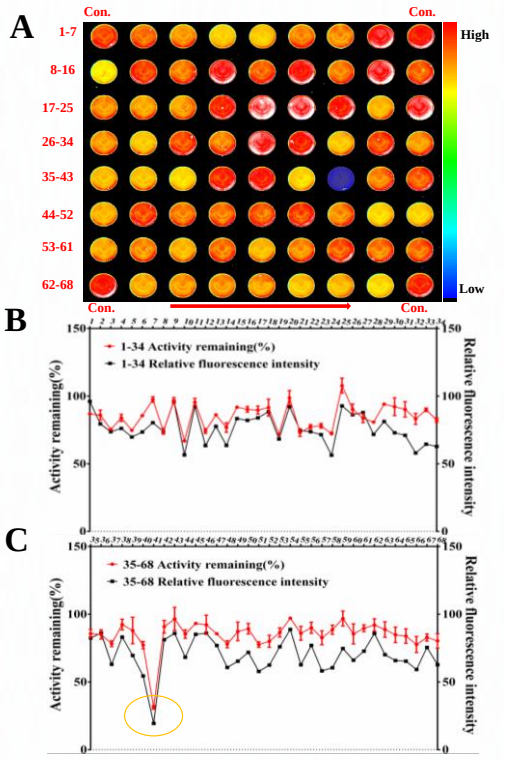

Figure 3. (**A**) Visual high-throughput fluorescence image of the inhibitory effects of 68 kinds of herbs toward FAAH assayed using **THPO**; (**B**, **C**) the inhibitory effects on FAAH measured using **THPO** by microplate reader (red, λ_{ex} 550 nm, λ_{em} 592 nm), and the remaining FAAH activity (black) based on the relative fluorescence intensity of fluorescence images (**A**) in each well of 96-well plate.

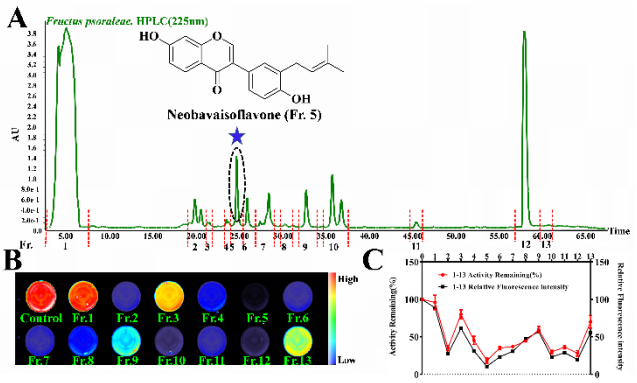

Figure 4. (**A**) HPLC fractions of *Psoralea corylifolia Linn.*; (**B**) fluorescence image of the inhibitory effects of 13 fractions separated from *Psoralea corylifolia Linn.* toward FAAH assayed using **THPO**; (**C**) the inhibitory effects on FAAH measured using a microplate reader (red, λ_{ex} 550 nm, λ_{em} 592 nm), and the remaining FAAH activity (black) based on the relative fluorescence intensity of fluorescence images (**B**) in each well of 96-well plate.

Interestingly, varying degrees of inhibitory effects were observed from different fractions. Briefly, among various fractions, **Fr. 5** exhibited the strongest inhibition toward FAAH when compared with the others, which produced a residual activity of 18.41% at a concentration of 2.5 μg/mL. Compared with **Fr. 5**, **Fr. 10** and **Fr. 12** displayed inhibition with residual

activity of 29.98% and 28.08%, respectively. While, other fractions including **Fr. 2**, **Fr. 4**, **Fr. 6**, **Fr. 7**, **Fr. 8** and **Fr. 9** all displayed less inhibition (residual activity > 35%). **Fr. 3** and **Fr. 13** exhibited a very weak inhibition (residual activity > 70%), **Fr. 1** had almost no inhibition activity.

Isolation and identification of the key inhibitory compound of Psoralea corylifolia Linn. toward FAAH. As shown in **Figure S16**, the inhibition activity of 13 fractions was also confirmed by the classic hydrolysis reaction of AEA. Consistent with the previous study, **Fr. 5** also exhibited a potent inhibitory activity on FAAH. Thus, the target compound (**L-BGZ**) in **Fr. 5** was isolated, next, on the basis of spectroscopic data, including ^{1}H NMR, ^{13}C NMR and HRMS; finally, **L-BGZ** was determined to be an isoflavone derivative possessing an isopentene group. (**Figure S17 – 19, Table S2**) Compared with the previously reported spectroscopic data, **L-BGZ** was determined to be Neobavaisoflavone. Next, the inhibitory effect of Neobavaisoflavone was evaluated. As shown in **Figure 5**, this novel natural inhibitor of FAAH exhibited much higher inhibition activity than Biochanin A, a previously reported natural inhibitor (IC_{50}: 131.6 ± 5.12 nmol *vs* 714.5 ± 44.13 nmol) toward FAAH. These results confirmed that **THPO** has great superiority in the screening of FAAH inhibitors and Neobavaisoflavone could serve as a novel natural FAAH inhibitor for further investigation of its biological function.

Molecular docking. To explore the potential binding model of Neobavaisoflavone and FAAH, molecular docking was performed using Discovery Studio 3.5 to provide an insight into any potential interactions. As presented in **Figure 6B** and **C**, Neobavaisoflavone could occupy the binding pocket. The hydroxyl group at the 7-position of Neobavaisoflavone could form a hydrogen bond with Thr488 located at the entrance of the active site, an important alpha helix. Another key hydrogen bond was observed between the B ring carbonyl group of Neobavaisoflavone and the side chain of Tyr194. The phenyl moiety (A ring) of Neobavaisoflavone initiated a Pi-Alkyl interaction with Leu404. Additionally, the B ring carbonyl group of Neobavaisoflavone of Y29 interacts with residues Ile238, Ser241 and Gly239, resulting in three key hydrogen bond interactions, which anchors the ligand in the binding pocket. While the isopentene group is deeply embedded in a hydrophobic pocket including Met191, Leu278, and Ile238 residues facilitated by hydrophobic interactions. The above results provide the structural basis for Neobavaisoflavone as a potent FAAH inhibitor.

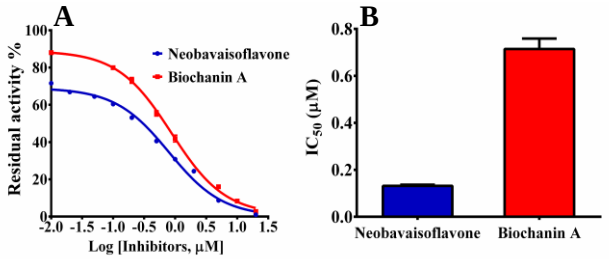

Figure 5. (**A**) The inhibitory effects of Neobavaisoflavone and Biochanin A with increasing concentration; (**B**) the IC_{50} values of Neobavaisoflavone and Biochanin A.

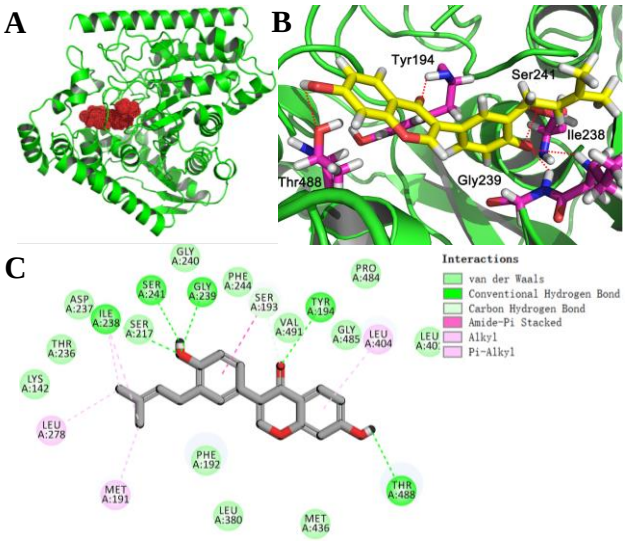

Figure 6. (A) The homology model of human FAAH; **(B)** Molecule docking of Neobavaisoflavone and FAAH; **(C)** Detaild for the interaction between Neobavaisoflavone and FAAH.

CONCLUSIONS

In summary, based on the catalytic mechanism of FAAH, we successfully developed a novel enzyme-activated fluorescent probe named **THPO** which possessing high selectivity and sensitivity toward FAAH among various enzymes. The kinetic parameters indicated that **THPO** had a very high affinity toward FAAH, which made it suitable in the measurement of FAAH activity in complex systems. Importantly, a visual high-throughput screening method for FAAH inhibitors was established using **THPO** and a novel natural efficient FAAH inhibitor Neobavaisoflavone was discovered and identified from 68 herb medicines. These results fully demonstrated the potential utility of **THPO** in investigating the physiological function of FAAH in living systems, as well as providing a novel method for the rapid screening of FAAH inhibitors with therapeutic potential for various diseases associated with FAAH.

ASSOCIATED CONTENT

Supporting Information

Synthetic procedures, NMR, HRMS-characterization, and Supplementary Figures for the experiments. The Supporting Information is available free of charge on the ACS Publications website.

AUTHOR INFORMATION

*****Corresponding Author

E-mail addresses: maxc1978@163.com (X. Ma), leifeng@dmu.edu.cn (L. Feng), and t.d.james@bath.ac.uk (T. D. James)

Author Contributions

# These authors contributed equally.

Notes

The authors declare no competing financial interests.

ACKNOWLEDGMENTS

The authors thank the National Natural Science Foundation of China (81930112, 81622047, 81503201and 21572029), National Science and Technology Major Project of the Ministry of Science and Technology of China (No. 2018ZX09735005), National Key R&D Program of China (2018YFC1705900), State Key Laboratory of Fine Chemicals (KF1803), Open Research Fund of the State Key Laboratory of Cognitive Neuroscience and Learning (CNLZD1801) for financial support. TDJ wishes to thank the Royal Society for a Wolfson Research Merit Award.

REFERENCES

(1) Boger, D. L.; Fecik, R. A.; Patterson, J. E.; Miyauchi, H.; Patricelli, M. P.; Cravatt, B. F., Fatty acid amide hydrolase substrate specificity. *Bioorg. Med. Chem. Lett.*, **2000**, *10*, 2613-2616.

(2) Piomelli, D., The molecular logic of endocannabinoid signalling. *Nat. Rev. Neurosci.*, **2003**, *4*, 873-884.

(3) McKinney, M. K.; Cravatt, B. F., Structure and function of fatty acid amide hydrolase. *Annu. Rev. Biochem.*, **2005**, *74*, 411-432.

(4) Cravatt, B. F.; Saghatelian, A.; Hawkins, E. G.; Clement, A. B.; Bracey, M. H.; Lichtman, A. H., Functional disassociation of the central and peripheral fatty acid amide signaling systems. *Proc. Natl. Acad. Sci.*, **2004**, *101*, 10821.

(5) Tuo, W.; Leleu-Chavain, N.; Spencer, J.; Sansook, S.; Millet, R.; Chavatte, P., Therapeutic potential of fatty acid amide hydrolase, monoacylglycerol lipase, and N-acylethanolamine acid amidase inhibitors. *J. Med. Chem.*, **2017**, *60*, 4-46.

(6) Lichtman, A. H.; Shelton, C. C.; Advani, T.; Cravatt, B. F., Mice lacking fatty acid amide hydrolase exhibit a cannabinoid receptor-mediated phenotypic hypoalgesia. *Pain*, **2004**, *109*, 319-327.

(7) Walker, J. M.; Huang, S. M.; Strangman, N. M.; Tsou, K.; Sanudo-Pena, M. C., Pain modulation by release of the endogenous cannabinoid anandamide. *Proc. Natl. Acad. Sci.*, **1999**, *96*, 12198-12203.

(8) N. Ueda, R. A. Puffenbarger, S. Yamamoto, D. G. Deutsch, The fatty acid amide hydrolase (FAAH). *Chem. Phys. Lipids.*, **2000**, *108*, 107-121.

(9) Muccioli, G. G., Endocannabinoid biosynthesis and inactivation, from simple to complex. *Drug Discov. Today*, **2010**, *15*, 474-483.

(10) Massa, F.; Marsicano, G.; Hermann, H.; Cannich, A.; Monory, K.; Cravatt, B. F.; Ferri, G. L.; Sibaev, A.; Storr, M.; Lutz, B., The endogenous cannabinoid system protects against colonic inflammation. *J. Clin. Invest.*, **2004**, *113*, 1202-1209.

(11) Di Venere, A.; Dainese, E.; Fezza, F.; Angelucci, B. C.; Rosato, N.; Cravatt, B. F.; Finazzi-Agro, A.; Mei, G.; Maccarrone, M., Rat and human fatty acid amide hydrolases: overt similarities and hidden differences. *Biochim. Biophys. Acta.*, **2012**, *1821*, 1425-1433.

(12) Chang, L.; Luo, L.; Palmer, J. A.; Sutton, S.; Wilson, S. J.; Barbier, A. J.; Breitenbucher, J. G.; Chaplan, S. R.; Webb, M., Inhibition of fatty acid amide hydrolase produces analgesia by multiple mechanisms. *Br. J. Pharmacol.*, **2006**, *148*, 102-113.

(13) Hohmann, A. G.; Suplita, R. L.; Bolton, N. M.; Neely, M. H.; Fegley, D.; Mangieri, R.; Krey, J. F.; Walker, J. M.; Holmes, P. V.; Crystal, J. D.; Duranti, A.; Tontini, A.; Mor, M.; Tarzia, G.; Piomelli, D., An endocannabinoid mechanism for stress-induced analgesia. *Nature*, **2005**, *435*, 1108-1112.

(14) Wei, B. Q.; Mikkelsen, T. S.; McKinney, M. K.; Lander, E. S.; Cravatt, B. F., A second fatty acid amide hydrolase with variable distribution among placental mammals. *J. Biol. Chem.*, **2006**, *281*, 36569-36578.

(15) Kathuria, S.; Gaetani, S.; Fegley, D.; Valino, F.; Duranti, A.; Tontini, A.; Mor, M.; Tarzia, G.; La Rana, G.; Calignano, A.; Giustino, A.; Tattoli, M.; Palmery, M.; Cuomo, V.; Piomelli, D., Modulation of anxiety through blockade of anandamide hydrolysis. *Nat. Med.*, **2003**, *9*, 76-81.

(16) Wollank, Y.; Ramer, R.; Ivanov, I.; Salamon, A.; Peters, K.; Hinz, B., Inhibition of FAAH confers increased stem cell migration via PPARalpha. *J. Lipid. Res.*, **2015**, *56*, 1947-1960.

(17) Kono, M.; Matsumoto, T.; Imaeda, T.; Kawamura, T.; Fujimoto, S.; Kosugi, Y.; Odani, T.; Shimizu, Y.; Matsui, H.; Shimojo, M.; Kori, M., Design, synthesis, and biological evaluation of a series of piperazine ureas as fatty acid amide hydrolase inhibitors. *Bioorg. Chem.*, **2014**, *22*, 1468-1478.

(18) Marco, E. M.; Rapino, C.; Caprioli, A.; Borsini, F.; Laviola, G.; Maccarrone, M., Potential therapeutic value of a novel FAAH inhibitor for the treatment of anxiety. *PloS one*, **2015**, *10*, e0137034.

(19) Ravi, J.; Sneh, A.; Shilo, K.; Nasser, M. W.; Ganju, R. K., FAAH inhibition enhances anandamide mediated anti-tumorigenic effects in non-small cell lung cancer by downregulating the EGF/EGFR pathway. *Oncotarget*, **2014**, *5*, 2475-2486.

(20) A. Lodola, R. Castelli, M. Mor, S. Rivara, Fatty acid amide hydrolase inhibitors: a patent review (2009-2014). *Expert Opin. Ther. Pat.*, **2015**, 25, 1247-1266.

(21) Jayamanne, A.; Greenwood, R.; Mitchell, V. A.; Aslan, S.; Piomelli, D.; Vaughan, C. W., Actions of the FAAH inhibitor URB597 in neuropathic and inflammatory chronic pain models. *Br. J. Pharmacol.*, **2006**, *147*, 281-288.

(22) Mileni, M.; Kamtekar, S.; Wood, D. C.; Benson, T. E.; Cravatt, B. F.; Stevens, R. C., Crystal structure of fatty acid amide hydrolase bound to the carbamate inhibitor URB597: discovery of a deacylating water molecule and insight into enzyme inactivation. *J. Mol. Biol.*, **2010**, *400*, 743-754.

(23) Huggins, J. P.; Smart, T. S.; Langman, S.; Taylor, L.; Young, T., An efficient randomised, placebo-controlled clinical trial with the irreversible fatty acid amide hydrolase-1 inhibitor PF-04457845, which modulates endocannabinoids but fails to induce effective analgesia in patients with pain due to osteoarthritis of the knee. *Pain*, **2012**, *153*, 1837-1846.

(24) Ning, J.; Liu, T.; Dong, P.; Wang, W.; Ge, G.; Wang, B.; Yu, Z.; Shi, L.; Tian, X.; Huo, X.; Feng, L.; Wang, C.; Sun, C.; Cui, J.; James, T. D.; Ma, X., Molecular design strategy to construct the near-infrared fluorescent probe for selectively sensing human Cytochrome P450 2J2. *J. Am. Chem. Soc.*, **2019**, 141, 1126−1134.

(25) Liu, H. W.; Chen, L.; Xu, C.; Li, Z.; Zhang, H.; Zhang, X. B.; Tan, W., Recent progresses in small-molecule enzymatic fluorescent probes for cancer imaging. *Chem. Soc. Rev.*, **2018**, *47*, 7140-7180.

(26) Ning, J.; Wang, W.; Ge, G.; Chu, P.; Long, F.; Yang, Y.; Peng, Y.; Feng, L.; Ma, X.; James, T. D., Target enzyme-activated two-photon fluorescent probes: a case study of CYP3A4 using a two-dimensional design strategy. *Angew. Chem. Int. Ed. Engl.*, **2019**, *58*, 9959-9963.

(27) Zhang, J.; Chai, X.; He, X. P.; Kim, H. J.; Yoon, J.; Tian, H., Fluorogenic probes for disease-relevant enzymes. *Chem. Soc. Rev.*, **2019**, *48*, 683-722.

(28) Wu, X.; Shi, W.; Li, X.; Ma, H., Recognition moieties of small molecular fluorescent probes for bioimaging of enzymes. *Acc. Chem. Res.*, **2019**, *52*, 1892-1904.

(29) Jin, Y.; Tian, X.; Jin, L.; Cui, Y.; Liu, T.; Yu, Z.; Huo, X.; Cui, J.; Sun, C.; Wang, C.; Ning, J.; Zhang, B.; Feng, L.; Ma, X., Highly specific near-infrared fluorescent probe for the real-time detection of β-glucuronidase in various living cells and animals, *Anal. Chem*., 2018, 90, 3276−3283.

(30) Feng L.; Ning J.; Tian X.; Wang C.; Zhang L.; Ma X.; James T.; Fluorescent probes for bioactive detection and imaging of phase Ⅱ metabolic enzymes. *Coord. Chem. Rev*., **2019**, *399*, 213026.

(31) Ramarao, M. K.; Murphy, E. A.; Shen, M. W.; Wang, Y.; Bushell, K. N.; Huang, N.; Pan, N.; Williams, C.; Clark, J. D., A fluorescence-based assay for fatty acid amide hydrolase compatible with high-throughput screening. *Anal. Biochem.*, **2005**, *343*, 143-151.

(32) Kage, K. L.; Richardson, P. L.; Traphagen, L.; Severin, J.; Pereda-Lopez, A.; Lubben, T.; Davis-Taber, R.; Vos, M. H.; Bartley, D.; Walter, K.; Harlan, J.; Solomon, L.; Warrior, U.; Holzman, T. F.; Faltynek, C.; Surowy, C. S.; Scott, V. E., A high throughput fluorescent assay for measuring the activity of fatty acid amide hydrolase. *J. Neurosci. Methods*, **2007**, *161*, 47-54.

(33) Huang, H.; Nishi, K.; Tsai, H. J.; Hammock, B. D., Development of highly sensitive fluorescent assays for fatty acid amide hydrolase. *Anal. Biochem.*, **2007**, *363*, 12-21.

(34) Adams, S. T., Jr.; Mofford, D. M.; Reddy, G. S.; Miller, S. C., Firefly luciferase mutants allow substrate-selective bioluminescence imaging in the mouse brain. *Angew. Chem. Int. Ed. Engl.*, **2016**, *55*, 4943-4946.

35) Mofford, D. M.; Adams, S. T., Jr.; Reddy, G. S.; Reddy, G. R.; Miller, S. C. Luciferin amides enable in vivo bioluminescence detection of endogenous fatty acid amide hydrolase activity. *J. Am. Chem. Soc.*, **2015**, 137, 8684-8687.

(36) Chen, B.; Lv, C.; Tang, X., Chemoselective reduction-based fluorescence probe for detection of hydrogen sulfide in living cells. *Anal. Bioanal. Chem.*, **2012**, *404*, 1919-1923.

(37) Xie, K.; Chen, R.; Li, J.; Wang, R.; Chen, D.; Dou, X.; Dai, J., Exploring the catalytic promiscuity of a new glycosyltransferase from Carthamus tinctorius. *Org. Lett.*, **2014**, *16*, 4874-4877.

(38) Brandvold, K. R.; Weaver, J. M.; Whidbey, C.; Wright, A. T., A continuous fluorescence assay for simple quantification of bile salt hydrolase activity in the gut microbiome. *Sci. Rep.*, **2019**, *9*, 1359.

(39) Tian, X. ; Yan, F. ; Zheng, J.; Cui, X.; Feng, L.; Li, S.; Jin, L.; James, T. D.; Ma, X., Endoplasmic reticulum targeting ratiometric fluorescent probe for carboxylesterase 2 detection in drug-induced acute liver injury. *Anal. Chem.*, **2019**, *91*, 15840-15845.
(40) Mileni, M.; Garfunkle, J.; DeMartino, J. K.; Cravatt, B. F.; Boger, D. L.; Stevens, R. C., Binding and inactivation mechanism of a humanized fatty acid amide hydrolase by alpha-ketoheterocycle inhibitors revealed from cocrystal structures. *J. Am. Chem. Soc.*, **2009**, *131*, 10497-10506.
(41) Yao, D.; Pan, D.; Zhen, Y.; Huang, J.; Wang, J.; Zhang, J.; He, Z., Ferulin C triggers potent PAK1 and p21-mediated anti-tumor effects in breast cancer by inhibiting Tubulin polymerization in vitro and in vivo. *Pharmacol. Res.*, **2020**, *152*, 104605.

Table of Contents (TOC):